Investigations on the effects of heater surface characteristics on the bubble waiting period during nucleate boiling at low subcooling

Sarker, D.; Ding, W.; Franz, R.; Varlamova, O.; Kovats, P.; Zähringer, K.; Hampel, U.;

Originally published:

October 2018

Experimental Thermal and Fluid Science 101(2019), 76-86

DOI: https://doi.org/10.1016/j.expthermflusci.2018.09.021

Perma-Link to Publication Repository of HZDR:

https://www.hzdr.de/publications/Publ-28109

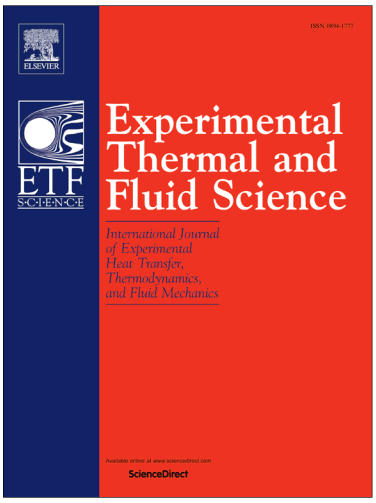

Investigations on the effects of heater surface characteristics on the bubble waiting period during nucleate boiling at low subcooling

D. Sarker, W. Ding, R. Franz, O. Varlamova, P. Kovats, K. Zähringer, U. Hampel

PII: S0894-1777(18)31088-4
DOI: https://doi.org/10.1016/j.expthermflusci.2018.09.021
Reference: ETF 9617

To appear in: *Experimental Thermal and Fluid Science*

Received Date: 11 June 2018
Revised Date: 5 September 2018
Accepted Date: 30 September 2018

Please cite this article as: D. Sarker, W. Ding, R. Franz, O. Varlamova, P. Kovats, K. Zähringer, U. Hampel, Investigations on the effects of heater surface characteristics on the bubble waiting period during nucleate boiling at low subcooling, *Experimental Thermal and Fluid Science* (2018), doi: https://doi.org/10.1016/j.expthermflusci.2018.09.021

Investigations on the effects of heater surface characteristics on the bubble waiting period during nucleate boiling at low subcooling

D. Sarker[a], W. Ding[a], R. Franz[a], O. Varlamova[c], P. Kovats[d], K. Zähringer[d], U. Hampel[a,b]

[a] Helmholtz-Zentrum Dresden-Rossendorf (HZDR), Institute of Fluid Dynamics, Bautzner Landstraße 400, 01328 Dresden, Germany
[b] Technische Universität Dresden, AREVA Endowed Chair of Imaging Techniques in Energy and Process Engineering, 01062 Dresden, Germany
[c] Experimentalphysik, Brandenburgische Technische Universität Cottbus-Senftenberg, 03046 Cottbus, Germany
[d] Lehrstuhl für Strömungsmechanik und Strömungstechnik, Otto-von-Guericke-Universität Magdeburg, 39016 Magdeburg, Germany

Abstract

In nucleate boiling the 'bubble waiting period', that is, the time duration between the departure of a grown bubble and the start of the formation of a new bubble from a cavity, plays a crucial role for the total heat transfer. Experiments were performed to study the influence of the heater surface characteristics on this parameter. A femtosecond pulsed laser was used to produce nano- and micro-patterned surfaces with roughness in the range of micrometers on stainless steel heater surfaces. Boiling experiments were conducted on a vertically oriented heater at atmospheric pressure and with degassed deionized water. Bubble generation, departure, sliding, detachment and inception of the next bubble have been recorded by high-resolution optical shadowgraphy. Bubble waiting periods were found to be longer for low-wettability smooth and rough surfaces. High-wettability rough surfaces showed a shorter bubble waiting period. The shortest (approximately 3 ms) and the longest (approximately 30 ms) bubble waiting periods were found for well-wetting surfaces with Sq =0.18 µm and for low-wetting surfaces with 0.12 µm, respectively. These corresponding roughness heights are denoted as 'optimal roughness heights'.

Keywords: bubble waiting period, surface wettability, roughness, vertical heater, nucleate boiling.

Nomenclature			
A	area (m²)	θ	liquid contact angle (°)
c_p, Cp	specific heat capacity (J kg^{-1} K^{-1}), heat capacity (Jkg^{-1})	σ	surface tension (N m^{-1})
d_w	bubble base diameter (m)	ρ	density (kg m^{-3})
D	diameter (m)		
f	bubble frequency (s^{-1})	*Subscripts*	
g	gravitational acceleration (= 9.81 m s^{-2})	act	activation
h	Heat transfer coefficient (Wm^{-2}K)	adv	advancing
h_{lv}	latent heat of evaporation (J kg^{-1})	conv	convective
k, K	thermal conductivity (Wm^{-1}K^{-1}), constant (dimensionless)	d	departure
X_{sm}	the mean width of surface profile dips (m)	eq	equivalent
N_n	nucleation site density (m^{-2})	ev	evaporation
Pr	Prandtl number (dimensionless)	hys	hysteresis
$\dot{q}$	heat flux (W m^{-2})	l	liquid
$\dot{Q}$	rate of heat flow (W)	ml	microlayer
Re	Reynolds number (dimensionless)	nb	nucleate boiling
S, Sq	suppression factor, root mean square roughness height of the surface (µm)	rec	receding
t	time (s)	refill	refilling
T	temperature (K)	sat	saturation
V	volume (m³)	tp	two-phase
		v	vapor
Greek symbols		w	heater wall, waiting period
δ	thermal liquid layer thickness (m)	x	normal to the heater wall
ΔP	Difference in vapor pressure corresponding to ΔT	y	upward direction
ΔT_{sub}	subcooling temperature (K)	∞	bulk

ΔT_w	wall superheat (K)		

1. Introduction

Nucleate boiling is an efficient mode of heat transfer which has numerous applications in heat transfer process engineering and has been widely investigated in the past. Further improvement of the boiling heat transfer in practical applications requires a more in-depth understanding of the fundamental physics of nucleate boiling. The visual perception of nucleate boiling is that of the so-called bubble ebullition cycle (Fig. 1). At a nucleation site, which is often assumed to be a small cavity with a minute amount of entrapped gas, a steam bubble starts growing once the critical thermodynamic conditions for evaporation are reached. At a certain point the balance of forces on the bubble leads to a departure from its position. The time t_d between the inception and departure of a growing steam bubble is referred to as the departure period. The time period t_w between the departure and the formation of a new bubble nucleus at the same site is referred to as bubble waiting period [1-3]. The bubble frequency $f=(t_w+t_d)^{-1}$ along with the nucleation site density N_n, the bubble departure diameter D_d and the latent heat of evaporation h_{lv} are the key parameters which make up the total evaporative heat flux

$$\dot{q}_{ev} = \frac{\pi}{6} D_d^3 \rho_v h_{lv} f N_n \qquad (1)$$

in nucleate boiling. Different groups found that the bubble waiting period is around 7.5 times [4, 5] and others, that it is more than 2 times [6, 7] longer than the departure period. Basu et al.[3] proposed a correlation for the waiting as a function of wall superheat ΔT_w in the form

$$t_w = 139.1\left(\Delta T_w^{-4.1}\right). \qquad (2)$$

The authors did not find significant dependency between subcooling and the bubble waiting period. Whereas Philips et al.[8] found that along with the wall superheat, liquid subcooling and thermal diffusivity had to be taken into account to predict the bubble waiting period. Other groups brought even more parameters into the discussion, e.g. bulk liquid velocity, heater surface characteristics, heat flux and others [9, 10]. Maity [11] reported that the bulk liquid velocity increase causes an increase in the bubble waiting time. In the next sections we will briefly summarize the findings from previous studies with a particular focus on the bubble waiting period and discuss the role of surface characteristics in detail from our point of view.

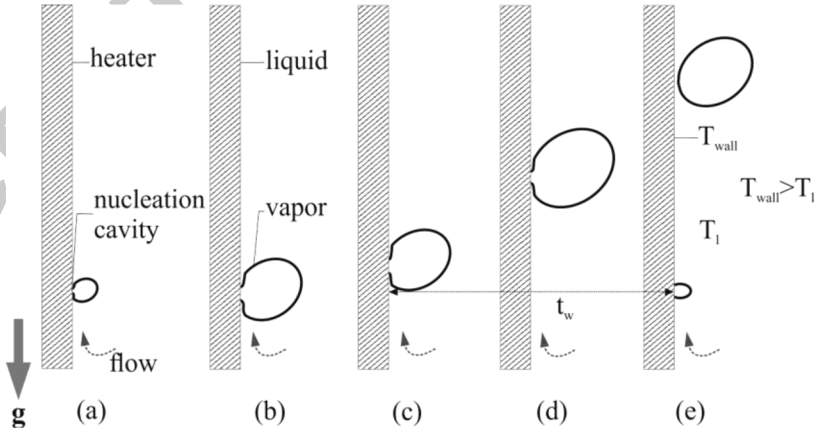

Fig. 1: Typical behavior of a nucleating steam bubble on a vertical heater wall. Left: (a) bubble nucleation, (b) bubble growth at the nucleation cavity, (c) having reached a critical size the bubble departs from its originating cavity, (d) the bubble slides a certain distance along the heater surface, (e) the bubble detaches from the wall and a new bubble is generated. The bubble waiting period is from c) to e).

1.1 Momentum and heat transfer in the thermal liquid layer during the bubble waiting period

Hsu and Graham's [1] analysis indicates that the waiting period is dependent on the surface cavity size, the bulk temperature of the fluid and the thermal boundary layer thickness δ. Their observation confirmed that when the bubble leaves the cavity, the fluid volume around the cavity is replenished by cold liquid. Then the liquid layer at the departed bubble base area is heated and the thermal layer is re-established in the vicinity of the bubble

nucleation site. The distortion of the thermal boundary layer during the bubble detachment was observed in different experiments [12-14]. Hsu and Graham also noted that the thermal layer recovery is dependent on the subcooling. Thus higher subcooling makes the waiting period quite longer than the bubble growth period. They assumed that fluid agitation is strong beyond the boundary layer and accurate prediction of waiting time is hence impossible unless this thermal layer is fully characterized. Fig. 2 shows the mechanistic concept of bubble instigation which is reproduced from Graham and Hendricks [15] and is based on the experimental findings of Hsu [16]. We see that temperatures of liquid layer and the thermal layer thickness (δ) increase with heater wall temperature (T_w) and they vary with time. According to Hsu [16], the nucleation proceeds only when the surrounding liquid is sufficiently warmer than the gas in the bubble. In another words, the bubble waiting period ends when the liquid temperature profile meets the critical bubble nucleation temperature. At this time, the thermal layer thickness also reaches a critical fraction of the bubble height (Fig. 2c). The heat transfer mechanisms from the heated wall to the bulk liquid through the thermal liquid layer influences the bubble inception. Amongst others, Ali and Judd [2] argued, that the growth of the thermal boundary layer and the subsequent bubble nucleation is governed by the combined effects of conductive and convective heat transfer to the liquid in the wake of rising bubbles. Haider and Webb [17] found out that the contribution of transient heat conduction is smaller compared to the transient convection.

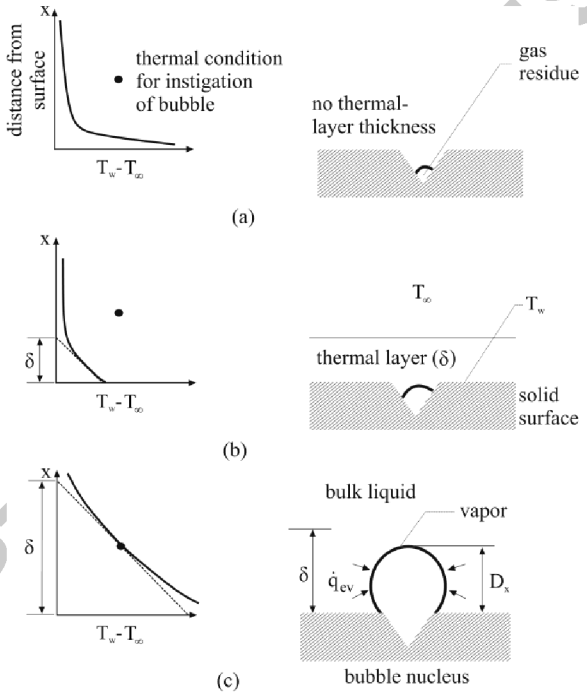

Fig. 2: History of thermal layer and bubble instigation (adapted from [15]); at the beginning of the waiting period (a), during the waiting period (b), end of the waiting period, beginning of the bubble growth (c).

Thermal fluid dynamics around a bubble has been studied in recent years as well. Yabuki et al. [18] employed high-speed digital interferometry to investigate the thermal field around an isolated steam bubble on a horizontal silicon surface. Their results showed that the superheated liquid on the heater surface mostly moves towards the nucleation site in planar direction during bubble departure. A column-like high temperature liquid wake was observed just below the rising bubble. But the temperature of the mixture of the bulk liquid and the superheated liquid did not increase significantly. Duan et al.[6] also observed a radially symmetric liquid velocity field towards the bubble base during the bubble growth period and typical vortices in the bubble wake upon the departure from the heater. Their findings show that agitation of liquid near the wall came to rest within ~10 ms after bubble departure while the total waiting period was about ~52 ms in horizontal pool boiling. According to them, the main effect of bubble departure on heat transfer is likely not micro-convection but rather the local displacement of the thermal boundary layer with the subsequent transient heat conduction during the waiting period. Other investigators noticed wake regions behind a sliding bubbles [19] as well and stated that the surface rewetting is a gradual process rather than a sudden quenching event and that the transient heat transfer process is distinctly different from any convection effect [20]. CFD analyses by Owoeye and Schubring [21] showed that, if the bulk liquid velocity rises, the temperature gradient around the bubble surface decreases.

1.2 Effects of surface characteristics on waiting time

The bubbling frequency was found higher while bubble sizes are smaller [22] and in general the bubble size negatively correlates with surface wettability [23, 24]. Phan et al. [9] found that for a static liquid contact angle between 30° to 70° waiting time does not change much. Waiting time starts to decrease when the static contact angle increases from 70° to 80° and waiting time increases significantly when the static liquid contact angle is below 30°. Moreover, when the heat flux increased from 220 to 300 kW/m², waiting time decreased by 70% whereas growth time decreased only by 23%. In the following we will delineate in detail the effects of surface characteristics on the bubble waiting period with reference to Figs. 3 (a, b, c).

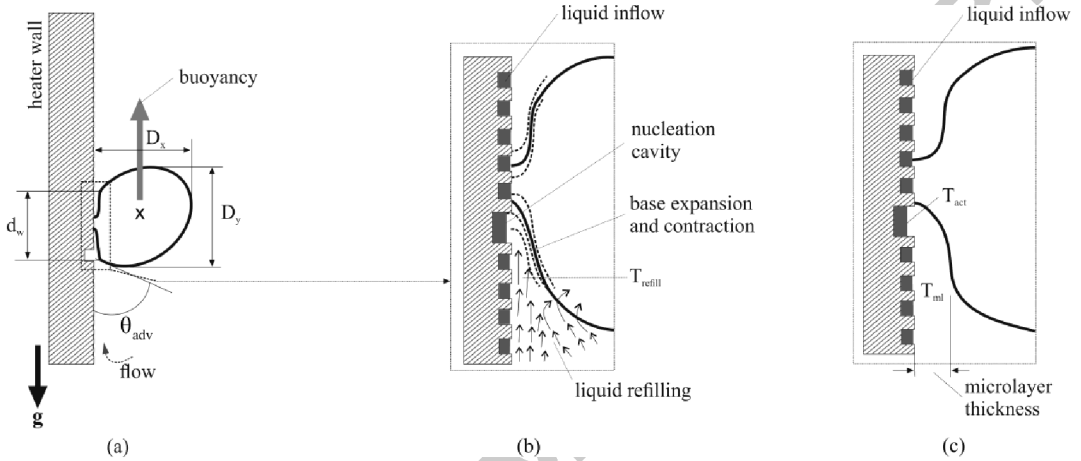

Fig. 3: a) Bubble geometry with center of mass ×, height D_x, width D_y, base diameter d_w and advancing contact angle θ_{adv}. b) Bubble base expansion and shrinkage, liquid circulation near bubble base. c) Liquid inflow through surface profile gaps and microlayer underneath the bubble base.

The surface roughness and wettability may affect the bubble waiting period by influencing the associated parameters of bubble dynamics, like bubble geometry, capillary force induced liquid velocity, sudden expansion and contraction of the bubble base due to the rapid evaporation of the microlayer, dynamic advancing contact angle, bubble sliding etc. Bubble sizes are represented here as bubble equivalent diameter $D_{eq}=\sqrt{D_x * D_y}$, with D_x being the bubble height and D_y the bubble width. For a single nucleation site we have a total rate of heat transfer

$$\dot{Q}_{ev,d}=\frac{\pi}{6}D_{eq,d}^3\rho_v h_{lv}\frac{1}{t_d}\propto\frac{D_{eq,d}^3}{t_d}. \quad (3)$$

$D_{eq,d}$ is the equivalent bubble diameter at departure. Heater surface characteristics have an effect on the total heat transfer via the term $D_{eq,d}^3/t_d$ (third term in eq. 3). Mukherjee and Kandlikar [25] commented that larger departing bubble diameters produce larger wakes and due to the shrinkage of a bubble base, a clockwise liquid circulation is created near the foot of a bubble which effectively pushes the superheated liquid away from the wall. Typically, a longer period of time is required to damp down the liquid motion in this case. The surface wettability plays an important role in rewetting the heater surface too. Generally, liquid spreads on the hydrophilic surfaces and beads on the hydrophobic surfaces [26]. Improved wettability decreases the liquid viscous drag along its flow path and thereby facilitates the liquid flow to the heated region [27]. Phan et al. [28] mentioned that surface wettability has an impact on frictional pressure drop due to the surface tension forces generated at the triple contact line.

A 'capillary wicking' is known as a spontaneous transport of a liquid into a porous system by capillary forces [29] which enhances the liquid supply and delays the irreversible growth of dry regions beneath bubbles [30]. The space between the structures can provide a large capillary pumping force bringing liquid back to the heated surface [27]. In the case of a perfectly smooth surface, there is no additional liquid supply to the bubble [31]. Few other experimental investigations supported the idea and suggested that by decreasing the surface profile gap size, the permeability of the micro-structured surface is reduced and the liquid inflow is amplified [32, 33]. This additional liquid supply may reduce the bubble waiting period. The effects of roughness on the superheated liquid layer outside the bubble projected area has been studied by Kim et al. [33]. They did not find any correlation between roughness and heat transfer coefficient for low wall superheat (5 K) as the boundary layer thickness (~100 μm) is

much larger than the profile height (10 … 40 µm). Zou et al.[34] reported the early evaporation of microlayer beneath the bubble base, the bubble growth rate and departure frequency due to the ridge height and spacing. Sriraman [35] argued that when the length of the nanofins exceeds the microlayer thickness this leads to a disruption of the microlayer and furthermore it increases the contact area between the liquid microlayer and the heater surface as well (Fig. 4). It can be added that if the surface roughness height is higher than the microlayer thickness, then the thickness of the liquid microlayer increases because the surface profile hinders the liquid movement and raises the heat transfer resistance [24]. A wave formation in the liquid microlayer is possible, when the capillary force is significant [36]. This effect may lead to the sudden expansion and contraction of the bubble base during bubble growth and departure (Fig. 3b). This in turn may cause additional disturbances to the surrounding liquid layer around the bubble base and influence the bubble waiting period.

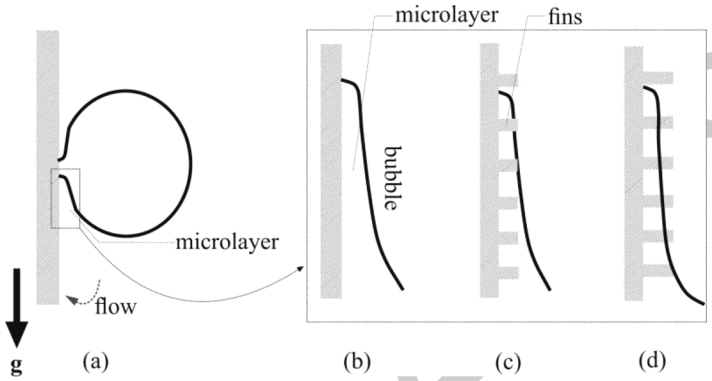

Fig. 4: Illustration of microlayer disruption by nanofins [35] (a). Left: (b) for a plain heater surface, (c) for a surface profile submerged in the microlayer, (d) for a partially submerged surface profile.

All the above studies clearly show that surface wettability and roughness influence the bubble growth and the departure process. The liquid refilling, regaining of the bubble nucleation conditions and consequently, the bubble waiting period are very much related to the bubble departure mechanism. Nano- and micro-scale surface roughness height, distance between profiles, and surface wettability may also affect the liquid penetration over the surface profile. However the effects of heater surface wettability and roughness on the bubble waiting period were yet reported widely in the previous works. To get a clearer view and quantitative conclusion, we investigated for surfaces with the root mean square roughness heights (Sq) in the range of 0.0041 µm to 0.46 µm for different wettability on a vertically orientated heater. The article is structured as follows. Section 2 introduces the test surface preparation and analyzing techniques, experimental setup, procedures, measurement techniques as well as the measurement uncertainties. Based on the detailed literature review and our understandings on the impacts of surface wettability and roughness on the bubble waiting period, section 3 discusses the experimental findings, that is, the effects of heat flux, surface roughness and wettability on the bubble waiting period for isolated bubbles in subcooled nucleate boiling. Section 4 eventually summarizes the results and gives a general outlook.

2. Experiment

We used stainless steel heater plates of 0.5 mm thickness in the experiment, as this is a widely used material in heat transfer applications. The thermal conductivity and the electrical resistivity of the material are 15 W/mK and 0.73 Ω mm/m at 20°C, respectively. The surfaces of the samples were treated in order to have different wettability and roughness. In earlier experiments, whose results are part of this analysis, we applied mirror polishing, wet-etching and self-assembling monolayer (SAM) coating. Thus we achieved the root mean square roughness heights of 0.004 µm (approx.) by mirror polishing, 0.099 µm and 0.46 µm by wet-etching. Details on this way of sample processing are given in [24] and a dedicate description of SAM process is given in [37]. The SAM coating was done with Heptadecafluorodecylphosphonic acid (CAS 80220-63-9) to produce hydrophobic surfaces. As the thickness of SAM coating is in the nanometer scale it does not influence the roughness but only the surface wettability. For the more recent experiments describe below, we used femtosecond pulsed laser treatment as a surface modification technique to produce a number of roughness heights of less than 5 µm. It helps to investigate the influences of surface roughness heights on the bubble growth rates in nucleate boiling more widely.

2.1 Surface preparation and analysis

The polished stainless steel surfaces were nano- and micro-structured in a 12 mm^2 area with linearly polarized pulsed laser light (wavelength 790 nm, pulse width approx. 100 fs, pulse rate 1 kHz, spot size 1.13 x 10^{-2} mm^2) from the available amplified Ti:Sapphire laser. To generate the laser induced period surface structures (LIPSS) at the irradiated area, a laser fluence exceeding the ablation threshold limit for the given material is required. In our experiment, we achieve this range of fluences by focusing the laser beam on the target. Thus the beam width was selected. The roughness of the LIPSS can be adjusted via laser scanning speed, pulse intensity and lateral overlapping of the scan lines. In our case we kept the laser power (1.15 J/cm²) and the overlapping (50%) constant and varied the scanning speed between 0.5 mm/s and 10 mm/s. At low irradiation power (1.15 J/cm² per pulse, 20 pulses per spot) homogeneous and regularly structured surface patterns of low roughness height were obtained while applying high irradiation power (1.15 J/cm² × 800 pulses/spot) leads to complex multiscale 3D patterns of higher roughness. More details of stainless steel surface preparation by femtosecond laser treatment can be found in Varlamova et al. [38]. Typical patterns for hydrophilic surfaces are nano-structured micro-islands separated by deep channels (Fig. 5a). Surfaces exhibiting hydrophobic properties are structured with fine ripples of lateral periods having low roughness (Fig. 5b).

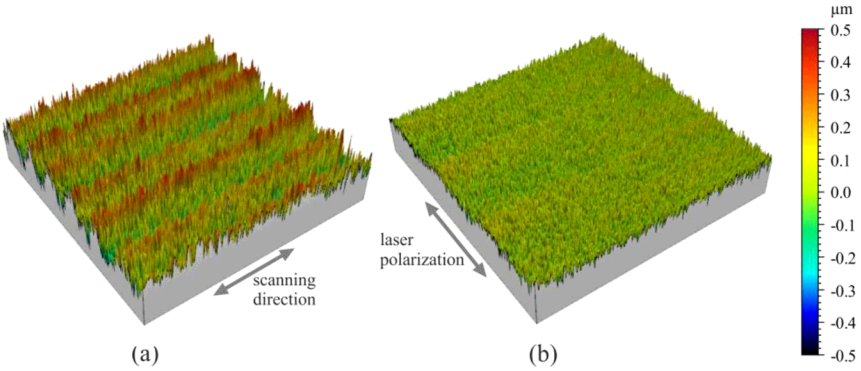

Fig. 5: 3D surface profiles of laser treated samples obtained from confocal microscopy. (a) hydrophilic surface structure produced with high irradiation dose, (b) hydrophobic surface structure produced with lower irradiation dose.

The surface topography was analyzed by non-contact confocal microscopy (µsurf explorer, xy-resolution: 0.3-3µm, z-resolution: 3 nm). The homogeneity of the surface roughness had been checked by imaging the surface topography at 6 different locations for each kind of preparation. The maximum deviation of the root mean square height of the surface was 5%. The advancing and the receding liquid contact angles (θ_{adv}, θ_{rec}) were measured using a goniometer (DataPhysics OCA 30) by the sessile drop method to represent the surface wettability. The difference between advancing and receding contact angle is known as the hysteresis liquid contact angle θ_{hys}. The maximum deviation of the hysteresis liquid contact angle was ±1.5°. Fig. 6 shows the averaged values of surface roughness and wettability were measured before and after performing the boiling experiment. Exemplary 2D surface profiles (samples 5 to 8) are shown in Fig. 7. The other surface profiles (samples 1 to 4) can be found in Sarker et al. [24]. To initiate boiling in a specific place on the sample a cylindrical cavity of size 1963.5 µm² and 50 µm depth was prepared by the micro-laser. The total size of the heater is 130 × 20 mm².

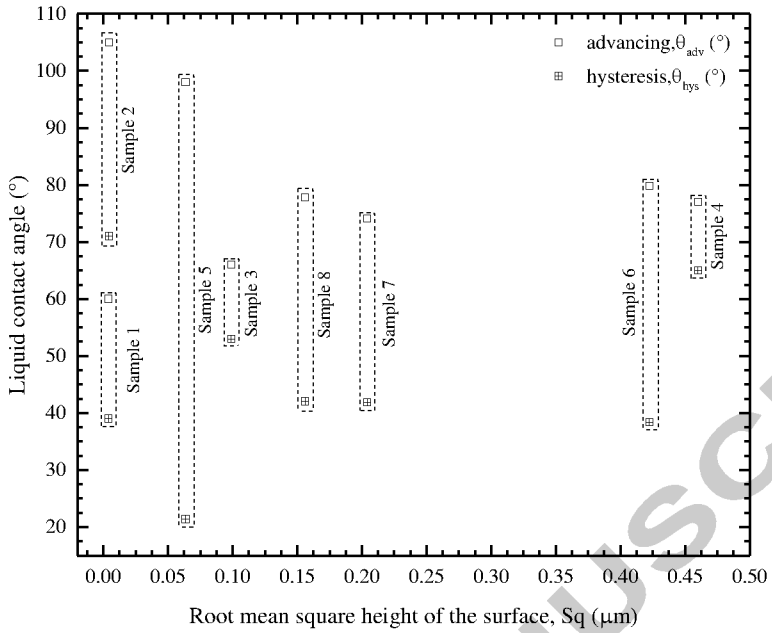

Fig. 6: Surface parameters of the prepared samples.

Samples 1 and 2 have a low roughness below 0.005 μm and the hysteresis liquid contact angles of these samples are 39° and 71° respectively. The hysteresis liquid contact angles of samples 1, 6, 7 and 8 are 40.50°±1.55°, whereas the root mean square height of these samples are 0.0041 μm, 0.422 μm, 0.204 μm and 0.156 μm, respectively. Effects of surface roughness on bubble waiting periods were investigated on these samples. The liquid hysteresis contact angles for samples 2, 3 and 4 are comparatively higher. Because sample 2 was coated with Heptadecafluorodecylphosphonic acid and samples 3 and 4 were wet-etched where wettability was decreased with the increase of roughness. Though sample 5 has a lower hysteresis liquid contact angle, the advancing liquid contact angle is more than 90°. Because the receding contact angle of this sample is higher than for other samples, wetting is lower. Therefore, investigations for low-wetting surfaces with different roughness heights were performed on samples 2, 3, 4 and 5.

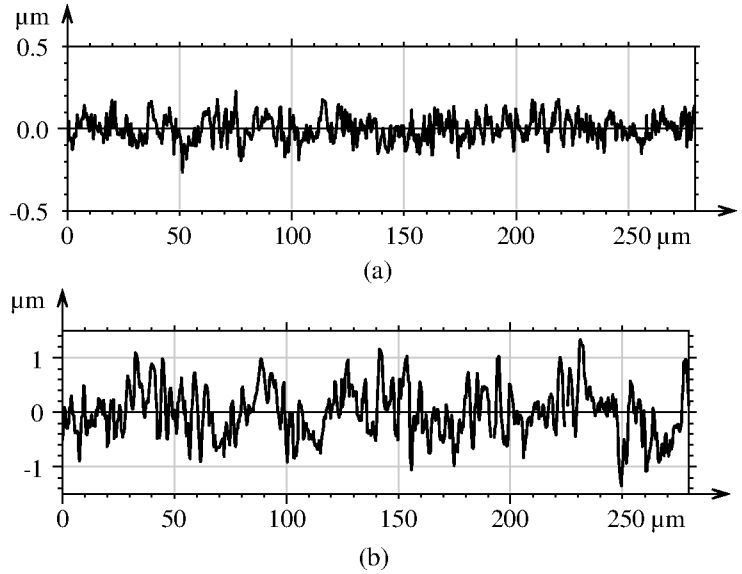

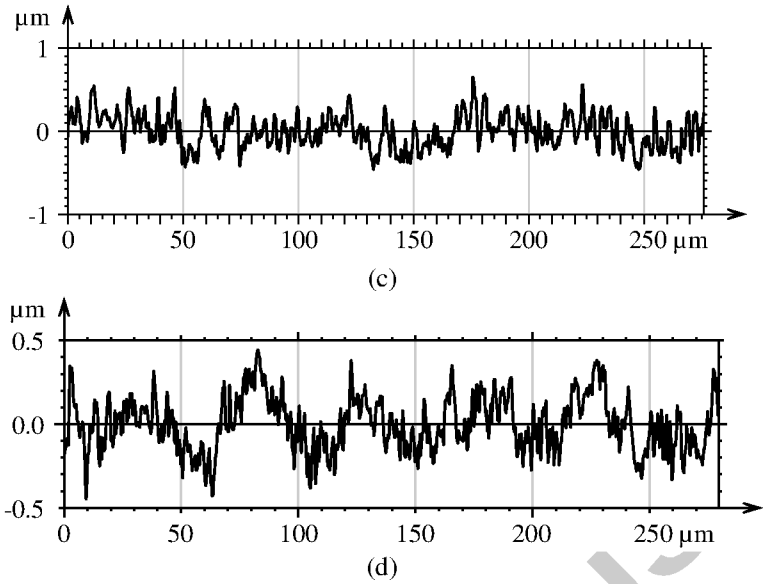

Fig. 7: 2D surface profiles of laser treated samples obtained from confocal microscopy. (a) Sq=0.064 µm, (b) Sq=0.422 µm, (c) Sq=0.204 µm, (d) Sq=0.156 µm.

2.2 Experimental procedure and measurement techniques

The boiling experiments were carried out in a borosilicate glass vessel (Fig. 8) at 1 bar. The liquid was deionized water. Before conducting the experiments, the glass vessel and test surfaces were cleaned properly. The glass vessel was cleaned by acetone and then rinsed with deionized water. Test surfaces were cleaned in an ultrasonic bath with ethanol at 40°C for 30 mins and subsequently dried by nitrogen gas. The deionized water in the loosely covered glass vessel was degassed by boiling it up to the saturation temperature and kept heating it at that temperature for at least 4 hours by an electric oven underneath the glass vessel. It was done to ensure the space above the water was filled with vapor and air may not get through to the water. Like other groups, Goel et al. [39]. and Kim et al. [31] also boiled the water up to 30 mins and 1 hour, respectively for degassing. The subcooling of the test liquid was maintained by the same electrical oven while performing the experiment. As indicated in Fig. 8, the glass wall had a rectangular opening at the heater side. The heater plates were tightly glued to that wall with a temperature-resistant silicon sealant (thermal conductivity 0.2 W/(mK)) such that the back-side of the heater could be directly accessed with an IR camera.

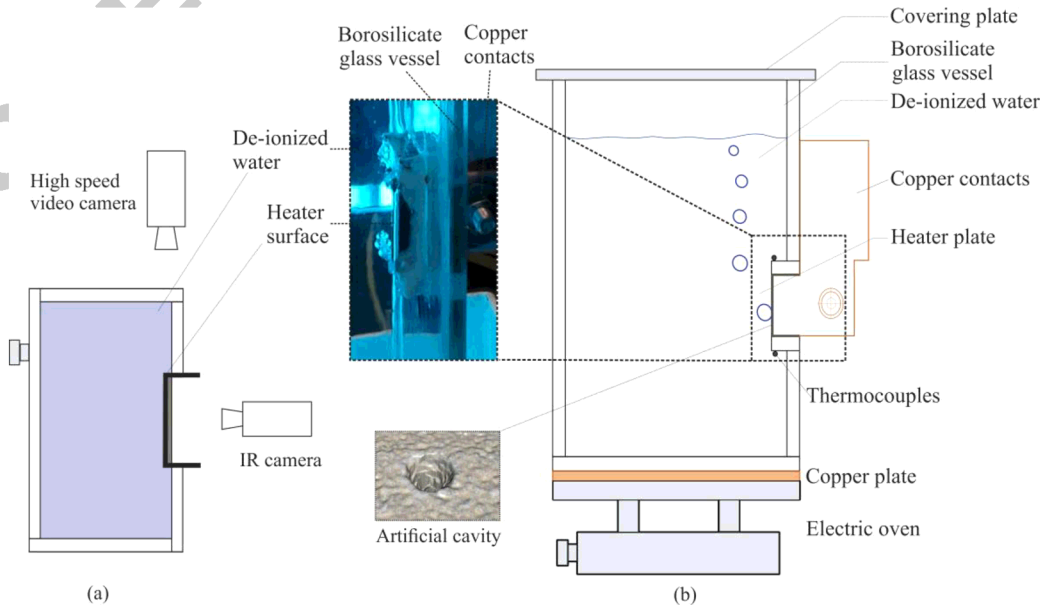

Fig. 8: Schematic of the test section top view (a) and side view (b).

An infrared (IR) camera (VarioCAM HD, 1024x768 pixels, ±1 K accuracy, frame rate 240 Hz) was used to measure the heater temperature distribution. The camera sensor captures the infrared radiation with the wavelengths from 7.5 to 14 μm which is reflected from the rear side of the heater plate. The camera sensor detects the intensity of infrared radiation and outputs the signal as pixel counts. The conversion of the radiation intensity to the temperature fields is done based on a counts-temperature calibration curve. The rear side of the plate was coated with the heat resistant black paint with an emissivity value of 0.93. For the calibration of IR measurements, a thermocouple was fixed on the heated plate. The maximum deviation between the IR and the calibrated thermocouple measurements was ±0.5 K. Since the thickness of the heater wall is 0.5 mm and the heater material is non-transparent, only the averaged temperature around the cavity area was recorded. IRBIS 3 professional was used to process and analyze the thermographic image sequences. Additionally we have calculated the inside temperature of the wall $\left(T_w=T_{sat}+\left(\frac{\dot{Q}}{A}-h_{conv}(T_w-T_l)\right)\frac{1}{h_{nb}}\right)$ using correlations (shown in Table 1) to verify our experimental results. Fig. 9 shows the calculated and experimentally measured temperatures. A combination of McAdam [40]'s and Chen [41]'s correlation for convective and nucleate boiling agrees well against the experimental results. The bulk liquid temperatures were measured by K-type thermocouples. Two K-type thermocouples were fixed above and below the heater in the bulk liquid in such a way that they did not influence the natural circulation flow of the liquid. All the thermocouples were calibrated and the deviation was found to be ±0.3 K. The test samples were directly heated via copper contacts. Experiments were conducted for the heat input rates in the range of 19 to 30 kW/m². The electrical power source has an uncertainty of around 1% and as the long connection cables produce some losses, we measured heating current and voltage directly at the connections of the heater plates. Furthermore we studied the liquid velocity fields generated by the heating with particle image velocimetry (PIV) technique using particles of 6.72 μm size stained with ethidium bromide as seeds in the liquid. We scanned the velocity field with 2400 Hz temporal and 13.22 μm/pixel spatial resolution. For each measurement, 500 frames were recorded and averaged them by the post-processing software LaVision DaVis 8.2.1. Thus the bulk liquid velocity due to the thermally induced buoyancy was determined in the range of 0.01 to 0.025 m/s near the heated samples. We compared these values with findings from Rousselet [42] who studied the effects of liquid velocity on the isolated bubble departure, lift-off and sliding for deionized water at 1 bar. With that we can estimate that the influences of buoyancy induced flow in the vessel on the bubble departure diameter, lift-off diameter and sliding velocity is less than 10%.

Table 1: Correlations for wall temperature calculation.

Authors	Correlations	Remarks
McAdams[40]	Convective boiling: $h_{conv}=0.0366Re^{0.80}Pr^{0.4}$.	For flat plate. Used in wider range of Reynolds number because of it's simplicity.
Chen[41]	Nucleate boiling: $h_{nb}=0.00122\left(\frac{k_l^{0.79}C_{pl}^{0.45}\rho_l^{0.49}}{\sigma_l^{0.5}\mu_l^{0.29}h_{lv}^{0.24}\rho_g^{0.24}}\right)\Delta T_{sat}^{0.24}\Delta P^{0.75}S$. $S=\frac{1}{1+2.53.10^{-6}Re_{tp}^{1.17}}$.	Re_{tp} is calculated for quality = 0. $\Delta T_{sat}=T_w-T_{sat}$.

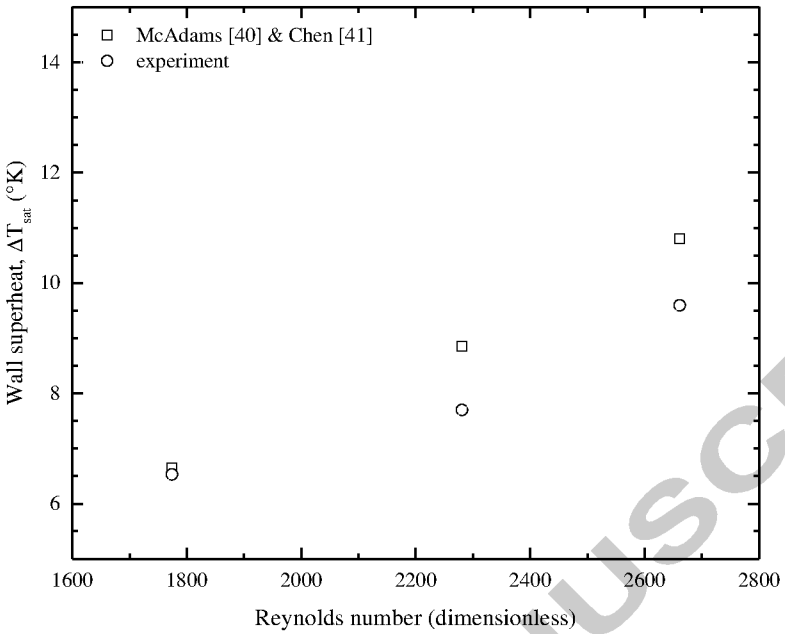

Fig. 9: Heater wall temperature on the low Reynolds number.

The bubble life cycle was recorded by high resolution optical shadowgraphy using a MotionPro high-speed video camera (1280x1024 pixels and 1030 frames per second) equipped with an AF Micro-Nikkor 105 mm f/2:8D lens and close-up macro filters of +5 diopters. During the experiments we recorded images with 2400 frames per second for samples 5, 6, 7 and 3000 frames per second for sample 8 (Sq=0.156 µm). The spatial resolution was 20.25 µm per pixel. The image processing software ImageJ was used to process the images from high speed video camera. During image processing, we subtracted the background, adjusted the threshold values, tracked the liquid-gas interface and filtered out the noise from the images to estimate the bubble sizes. Bubble base diameters were determined by tracking the temporal evolution of the bubble-solid interfaces. The spatial uncertainty of the imaging technique was estimated from the pixel resolution as ±0.036 mm and on the geometrical measurements of bubble sizes is ±0.02 mm. The bubble waiting period was determined by averaging around 20 life cycles. We calculated that that around 70% of data lies within one standard deviation in all experiments and one standard deviation is 1.06 ms. In the result section the averaged bubble waiting period is given. The bubble waiting period results for sample 1 to 4 were taken from the previous experimental studies [24].

3. Results and discussion

Figure 10 summarizes the bubble waiting periods for all the investigated samples and heat fluxes. The observations can be summarized as follows:

1. Bubble waiting periods reduce with the increase of heating rate. This is in agreement with the results of Phan et al.[9], Ali and Judd [2] and Euh et al. [43], who further found an increase of bubble departure frequency with the increasing of heat flux at 175 kPa and 300 kPa pressure.
2. Bubble waiting periods are generally longer for low-wetting surfaces.
3. There is an opposite trend for well- and low- wetting surfaces. For well-wetting surfaces t_W is minimum around Sq=0.18 µm. For low-wetting surfaces t_W is maximum around Sq=0.10µm.

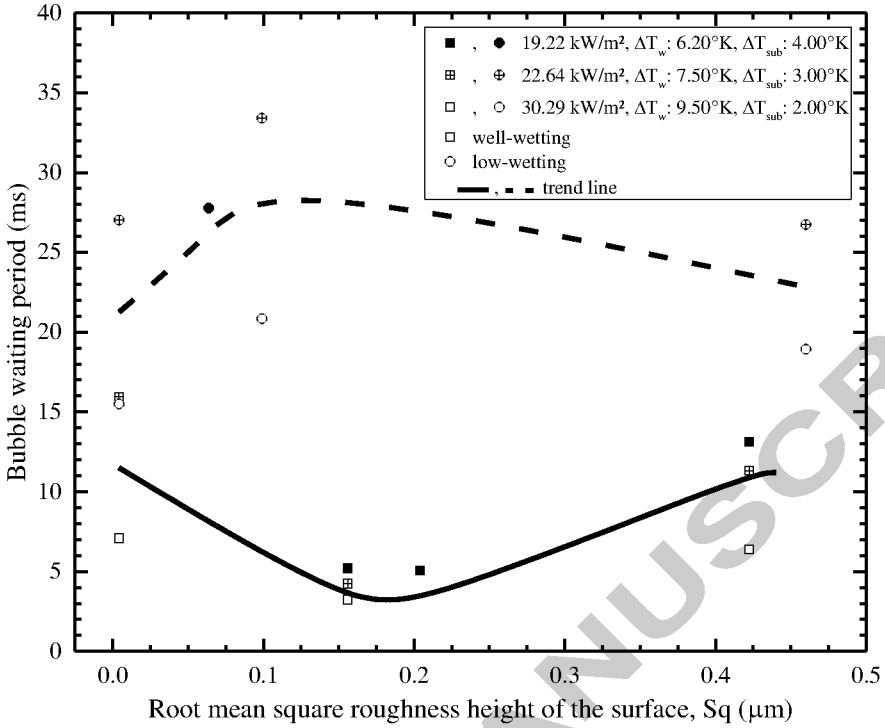

Fig. 10: Bubble waiting periods for different samples and heat fluxes.

The bubble waiting periods follow the distinguishable trend lines for different surface wettability and roughness in spite of the impact of the wall heating rate. The heating rate does not alter the effects of surface characteristics on the bubble waiting periods. If the applied heat transfer to the wall is greater, the wall superheat temperature becomes higher. Hence the temperature of the refilling liquid is also higher. A bubble nucleus begins to grow on the heating wall when the surrounding liquid is sufficiently superheated [16]. The heat required to activate a nucleation cavity is given by

$$\dot{Q}_l = \rho_l V_l c_{p,l} \frac{\Delta T}{\Delta t} = \rho_l K \left(\frac{\pi d_{w,d}^2}{4} \delta_l \right) c_{p,l} \frac{(T_{act} - T_{refill})}{\Delta t}. \quad (4)$$

Here V_l is the volume of the thermal liquid layer which is represented as factors of the thermal boundary layer thickness (δ_l) and the bubble base area during departure ($\frac{\pi d_{w,d}^2}{4}$), ΔT is the difference between the cavity activation temperature (T_{act}) and the adjacent liquid layer (T_{refill}) near the wall which needs to be reheated, Δt is the time period requires to reach the temperature difference ΔT, K is a constant that defines the bubble influential area as a multiple of the bubble base area. The temperature of refilling liquid (T_{refill}) increases with $\dot{Q}_l$. Therefore ΔT decreases and shorter time period Δt is required to activate the cavity for a constant bubble base diameter. Thus we can say that higher heat transfer expedites the reconstruction of the thermal liquid layer and reduces the time period for the inception of successive bubbles. The near wall liquid velocities during bubble departure (around 0.126 m/s [19], 0.25 m/s [25]) reported by different groups were much higher than the bulk liquid velocities measured (0.01~0.025m/s) in our experiment. Therefore we assumed that bulk liquid velocities do not play a significant role in the displacement of the superheated liquid layer in this study. Below we will explain the logical reasoning of the effects of surface wettability and roughness on bubble waiting periods in section 3.1 and 3.2, respectively.

3.1 Effects of surface wettability

The evaporative heat transfers through a bubble during departure can be qualitatively represented by $D_{eq,d}^3/t_d$ (Eq.3). The colder liquid fills the area vacated by the departing bubble and the newly formed liquid layer has to regain the same amount of heat which is carried away by departing bubbles for the cavity reactivation. The larger the recovered heat, the longer the waiting period. It has been postulated earlier that the liquid inflow towards the departing bubble base area is induced by bubble sizes, surface wetting characteristics etc. All these parameters influence the recovering of the distorted superheated thermal liquid layer and we investigate them here. Fig. 11

gives an indication of the heat extraction by bubbles in the course of departure. Fig. 12 shows the bubble equivalent diameters for well- and low-wetting surfaces and for different roughness heights during departure. The solid and dashed lines of these figures are best fitted curves derived from our experimental results using B-spline curve fitting method.

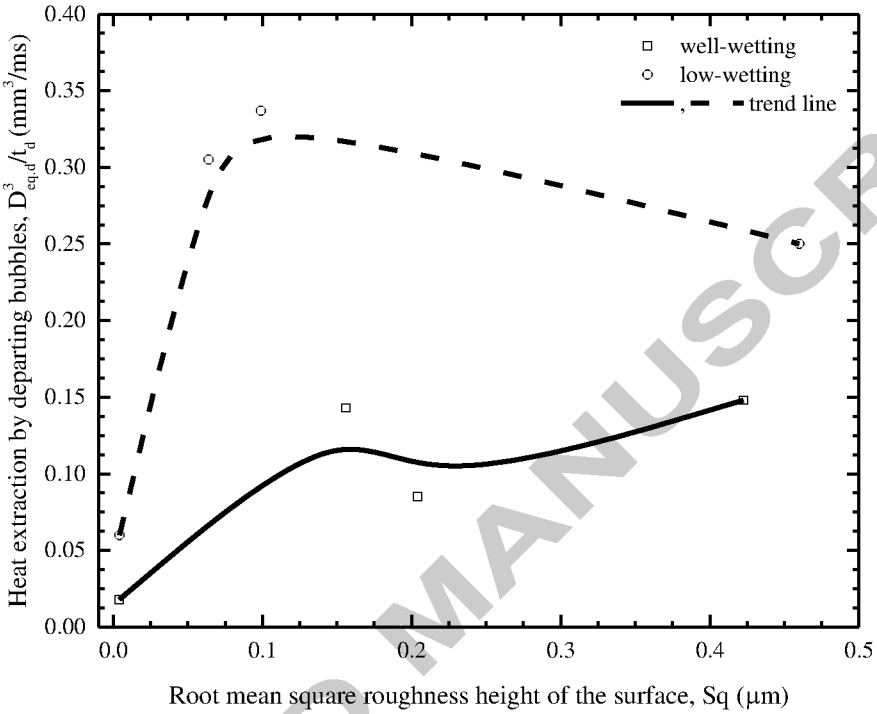

Fig. 11: Heat extraction by bubbles on well- and low- wetting surfaces.

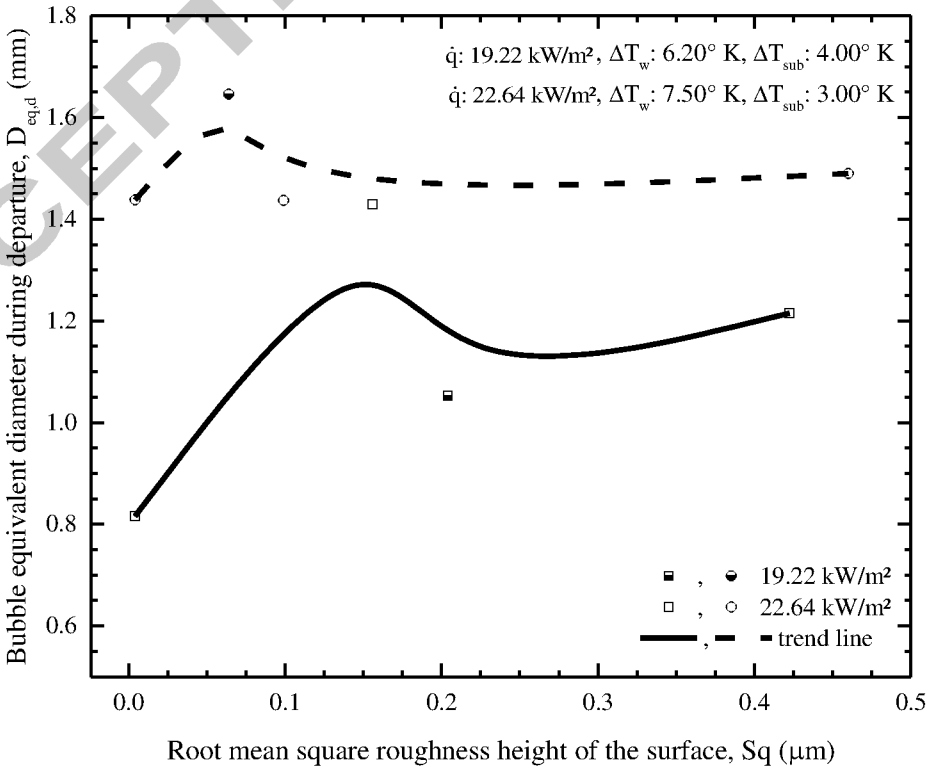

Fig. 12: Bubble equivalent diameter during departure for well- and low- wetting surfaces.

We can see that the heat extraction from the superheated liquid layer by departing bubbles is generally greater for low-wetting surfaces than for well-wetting surfaces (Fig. 11). Furthermore, heat extraction rates are maximum at the optimal roughness for low-and well-wetting surfaces, as the microlayer evaporation rates could be maximum in these cases. Our experimental results show that higher surface wettability generally leads to smaller bubble equivalent diameter during departure (Fig. 12). Bubble equivalent diameters during departure are from 0.8 mm to 1.4 mm and from 1.4 to 1.7 mm (Figs. 12) for high and low-wetting surfaces respectively. This is because, for low-wetting surfaces, surface tension forces act towards the outside of the bubble base. Larger departing bubble diameters bring a larger amount of liquid with a vortex structure towards the heater wall. Liquid circulation due to the larger vortex moves the superheated liquid away from the wall as well [25]. Therefore it requires a longer period of time to regain the cavity activation condition as we can see this in Fig. 10.

Furthermore, the heater surface characteristics affect the liquid inflow and consequently, the restoration of the superheated liquid layer. For example, the bubble departure diameters are similar (≈1.4 mm) for sample 2 (Sq=0.0042 μm, θ_{hys}=71°), sample 4 (Sq=0.46 μm, θ_{hys}=65°) and sample 8 (Sq=0.156 μm, θ_{hys}=42.05°), while the corresponding heat extraction rate ($D_{eq,d}^3/t_d$) are 0.06, 0.25 and 0.143 mm³/ms. Still the bubble waiting period is longer for sample 2, i.e. 27.02 ms, on the other hand for sample 4 and sample 8, they are 26.73 ms and 5.05 ms. This is because, the surface wettability is lower (θ_{hys}=71°) for sample 2 than that of sample 4 (θ_{hys}=65°) and sample 8 (θ_{hys}=42.05°). The liquid inflow gets influenced due to the capillary effects and Washburn [44] defined the capillary pressure by the term $\left(\frac{2\sigma\cos\theta}{0.5X_{sm}}\right)$. There θ is the liquid contact angle and X_{sm} represents the distance between the consecutive surface profile peaks. If X_{sm} reduces, the frictional loss increases. Therefore the liquid inflow velocity reduces with the increase of liquid contact angle for smooth surfaces of minimum profile gap. As a result the bubble waiting period is longer for a larger hysteresis liquid contact angle on smooth surfaces. These findings suggest that along with the surface roughness, the surface wettability plays role in the liquid movement during recovering of the superheated liquid layer. More on the impacts of surface roughness is shown in section 3.2.

3.2 Effects of surface roughness

Roughness effects on the bubble waiting periods were investigated for surfaces with the root mean square roughness height in the range of 0.0041 μm to 0.422 μm for well-wetting surfaces (θ_{hys}=40.50°±1.55°) and for low-wetting surfaces, the roughness heights are in the range of 0.0042 μm to 0.46 μm. Bubble departure diameters and heat extraction rates by bubbles are generally smaller for smooth surfaces than for rough surfaces. Comparatively larger bubble departure diameters and heat extraction rates are reported in between roughness heights of 0.0992 μm and 0.156 μm than that of the most rough surfaces (Sq=0.422 μm, 0.46 μm) both for well- and low-wetting surfaces. Since the heat extraction rates and bubble departure diameters are greater for these samples, there is a possibility also that the thermal liquid layer recovery period will also be longer for these samples. Fig. 10 shows that though this criterion is followed for low-wetting surfaces, well-wetting surfaces have additional effects. The extended surface profiles of rough surfaces introduce supplementary effects in regaining the thermal liquid layer. Hence bubble waiting periods for different roughness heights, reported in Fig. 10 cannot be characterized only considering bubble heat extraction rates and bubble sizes during departure.

Fig. 7 shows the periodic wavy structures in sample 6 (Sq=0.422 μm) and sample 8 (Sq=0.156 μm). Widths of these surface profiles' valleys are almost 50 μm and profile heights are 2 μm and around 1 μm for sample 6 and 8, respectively. According to the Washburn's [44] derivation, the valleys of the wavy surface enhance the additional liquid inflow to the departed bubble base area due to the capillary effects. The liquid inflow velocity is a function of capillary driven pressure and the frictional loss due to the surface profile. Different studies suggested that the liquid inflow velocity is maximum for the profile space between 20-60 μm and a gap below 10-20 μm the flow resistance increases that the inflow velocity sharply decreases [27, 33]. Thus, it can be predicted that the liquid inflow velocity is much greater for sample 6 (Sq=0.422 μm) and 8 (Sq=0.156 μm) than that of the smooth surface, since the profile gap of these samples is around 50 μm. Smooth surfaces do not allow additional liquid supply to the bubble. Therefore despite of smaller bubble sizes and the evaporative heat absorption rate ($D_{eq,d}^3/t_d$) for sample 1 (Sq=0.0041 μm), the liquid refilling on this surface is less compare to wavy structured surfaces. As a result, rebuilding of the thermal liquid layer is accelerated for wavy samples and the bubble waiting period reduces.

Additionally, the interaction between surface roughness and microlayer beneath the bubble base resembles the role of effective microlayer thickness on the initial bubble expansion rate [24] and bubble departure diameter. An extended area of rough surfaces generally increases the actual heat transfer area and accelerates the heating up of

the microlayer. The surface profile may get fully or partially submerged within the microlayer depending on the thickness of the liquid layer and the surface profile height. The faster initial bubble expansion rates for sample 8 (Sq=0.156 μm) (Fig. 13a) suggests that the effectivity of microlayer evaporation is greater for these surfaces. Plesset and Prosperetti [45] commented that "*if initial microlayer thickness is small for the wall to be effective, the liquid temperature of the microlayer recovers before the bubble collapse and reaches its initial value of wall temperature very rapidly just before microlayer dryout. For larger values of initial microlayer thickness, however the microlayer surface temperature remains close to the boiling point throughout most of the bubble lifetime*". On these grounds it can be said that the wall temperature recovery is speedy for the most effective microlayer thickness and a cavity gets activated earlier which we also observed for sample 8 (Sq=0.156 μm).

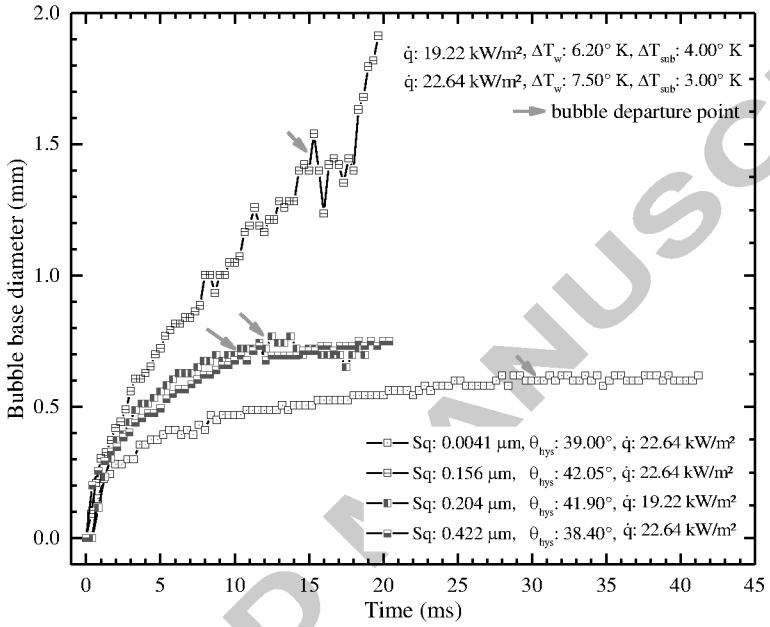

(a)

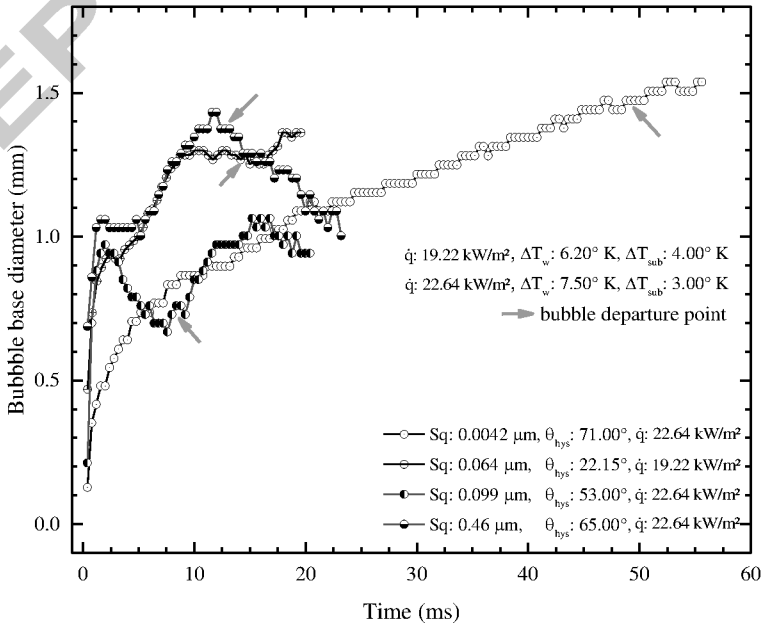

(b)

Fig. 13: Temporal evolution of bubble base diameter for well-wetting (a) and low-wetting (b) surfaces.

Surface roughness heights have further influence on bubble waiting period due to expansion and contraction of bubble bases during bubble growth and departure. For well-wetting surfaces, we did not observe major shrinkage effects during departure (Fig. 13a). The fluctuation in bubble base diameter can be seen after the departure of bubble from its nucleation cavity for sample 8 (Sq=0.156 μm). This is because just after the departure from the cavity new tiny bubbles generate and merge with departed large bubble. Expansion and contraction of bubble bases are reported for low-wetting rough surfaces (Fig. 13b). Because of these effects, waves propagate in the thermal liquid layer near the bubble base and the refilling liquid gets disturbed. As a result, the re-establishment of thermal liquid layer requires more time than for smoothly growing bubble bases. This kind of phenomenon was postulated earlier (Fig. 3b). The expansion and contraction in the bubble base during the bubble growth and the departure are presumably because of the microlayer evaporation and the movement of liquid into the microlayer. Bubble waiting periods for sample 4 (Sq=0.46 μm) and 5 (Sq=0.064 μm) are very close to each other (Fig. 10). In Fig. 13 (b) we see that the expansion of the bubble base is hindered within 5 ms of bubble generation and bubbles do not expand. No contraction effects have been found for these samples as well. After 5 ms, both bubble base diameters start to expand rapidly and push the surrounding liquid of the bubble base away. Sample 3 (Sq=0.099 μm) shows the maximum bubble waiting period in Fig. 10 and extracts the largest amount of heat (Fig. 11). Going back to Fig. 13 (b) we see that sample 3 (Sq=0.099 μm) first shows a large contraction in bubble base and then it starts to expand. We have also observed that the bubble advancing contact angle during departure is smaller for larger contraction for sample 3(Sq=0.099 μm). Thus we can assume that these shrinkage and expansion effects create additional disturbance in the surrounding liquid, which is stronger than that of samples 4 (Sq=0.46 μm) and 5 (Sq=0.064μm). Consequently, the bubble waiting period is much higher for sample 3 (Sq=0.099μm).

Summary and conclusions

This experimental study was focused to investigate the surface characteristics, especially wettability and roughness effects, on the bubble waiting periods for subcooled nucleate pool boiling on vertical surfaces. Stainless steel was used as heater material, degassed-deionized water was used as test medium and the experiment was conducted at 1 atmospheric pressure. The bubble waiting period was investigated on the heater surfaces of different wettability and roughness. In summary, the following results were obtained:

(i) Bubble waiting periods are generally greater over low-wetting surfaces.

(ii) Surface roughness extends the heat transfer area beneath the bubble base and allows liquid to inflow through channels over surfaces by the capillary effect. Thus it also enhances the reconstruction of the thermal liquid layer. Consequently bubble waiting periods are shorter for well-wetting rough surfaces compared to smooth surfaces.

(iii) The expansion and shrinkage effects are observed on bubble base during the bubble growth over low-wetting rough surfaces which may propagate disturbances in the surrounding liquid layer around the bubble base. This increases the bubble waiting period.

(iv) Bubble waiting periods are mostly lower for the well-wetting rough surfaces.

(v) Bubble waiting periods are found 3 ms (approx.) for well-wetting surfaces of Sq=0.18μm and 30 ms(approx.) for low-wetting surfaces of Sq=0.12μm.

The systematic study on the influences of associated bubble dynamics, namely bubble equivalent diameter, energizing the superheated liquid layer, liquid inflow to the departed bubble base area, microlayer evaporation etc. on bubble waiting periods are not widely reported in open literatures. The present work attempted to unfold the impact of surface wettability, roughness and surface profile etc. on the associated parameters of bubble dynamics and their influences on the bubble waiting period. The qualitative findings of this investigation can help to develop a more physics-based model of the bubble waiting period by capturing the surface characteristics effects. As well as, the results of this investigation can help to the design the heater surfaces with systemic combination of roughness and wettability which will increase the frequency of nucleated bubbles and the boiling heat transfer performance.

Acknowledgments

The authors like to thank Dr. Astrid Drechsler and Dr. Ralf Helbig from IPFDD and Mr. Heiko Pietruske, FWDF (HZDR) for their support in the experiment.

Conflict of interest

There is no conflict of interests.

Appendix

Table 2
Experimental samples with their respective surface parameters

Sample no.	Surface profile		Surface wettability		
	Root mean square roughness height of the surface (Sq) (µm)	Maximum roughness height of the surface (St) (µm)	Advancing (θ_{adv}) (°)	Receding (θ_{rec}) (°)	Hysteresis (θ_{hys}) (°)
01	0.00408	0.128	60	21	39
02	0.00424	0.144	105	34	71
03	0.099	0.821	66	13	53
04	0.46	3.54	77	12	65
05	0.0637	0.459	97.97	76.56	21.41
06	0.4224	2.7554	79.82	41.46	38.36
07	0.204	1.375	74.13	32.22	41.90
08	0.156	0.992	77.85	35.80	42.50

References

[1] Y. Y. Hsu, R. W. Graham, An analytical and experimental study of the thermal boundary layer and ebullition cycle in nucleate boiling. 1961, National aeronautics and Space Administration.
[2] A. Ali, R. L. Judd, An analytical and experimental investigation of bubble waiting time in nucleate boiling. Journal of Heat Transfer, 1981. **103**: p. 673-678.
[3] N. Basu, G. R. Warrier, V. K. Dhir, Wall Heat Flux Partitioning during Subcooled Flow Boiling: Part 1 - Model Development. Journal of Heat Transfer, 2005. **127**: p. 131-140.
[4] C. Gerardi, J. Buongiorno, L.W. Hu, T. McKrell, Study of bubble growth in water pool boiling through synchronized, infrared thermometry and high-speed video. International Journal of Heat and Mass Transfer, 2010. **53**(19-20): p. 4185-4192.
[5] S.B. Jung, H.D. Kim, An experimental method to simultaneously measure the dynamics and heat transfer associated with a single bubble during nucleate boiling on a horizontal surface. International Journal of Heat and Mass Transfer, 2014. **73**: p. 365-375.
[6] X. Duan, B. Phillips, T. McKrell, J. Buongiorno, Synchronized High-Speed Video, Infrared Thermometry, and Particle Image Velocimetry Data for Validation of Interface-Tracking Simulations of Nucleate Boiling Phenomena. Experimental Heat Transfer, 2013. **26**: p. 169-197.
[7] T. Yabuki, O. Nakabeppu, Heat transfer mechanisms in isolated bubble boiling of water observed with MEMS sensor. International Journal of Heat and Mass Transfer, 2014. **76**: p. 286-297.
[8] B. Philips, J. Buongiorno, T. McKrell. Nucleation site density, bubble departure diameter, wait time and local temperature distribution in subcooled flow boiling of water at atmospheric pressure. in The 15th International Topical Meeting on Nuclear Reactor Thermal Hydraulics. 2013. Pisa, Italy.
[9] H.T. Phan, N. Caney, P. Marty, S. Colasson, J. Gavillet, Surface wettability control by nanocoating: The effects on pool boiling heat transfer and nucleation mechanism. International Journal of Heat and Mass Transfer, 2009. **52**: p. 5459-5471.
[10] I. C. Chu, H. C. No, C.H. Song, Bubble lift-off diameter and nucleation frequency in vertical subcooled boiling flow. Journal of Nuclear Science and Technology, 2011. **48**(6): p. 936-949.
[11] S. Maity, Effect of velocity and gravity on bubble dynamics, California University of, Editor. 2000.
[12] R. C. Hendricks, R. R. Sharp, Initiation of cooling due to bubble growth on a heating surface. 1964, National Institute and Space Administration: Lewis Research Center, Ohio.

[13] Y. M. Chen, F. Mayinger, Measurement of heat transfer at the phase interface of condensing bubbles. International Journal of Multiphase Flow, 1992. **28**(6): p. 877-890.

[14] F. Mayinger. Advanced experimental methods. in International Conference on Convective Flow Boiling. 1995. Alberta, Canada: Taylor & Francis.

[15] R. W. Graham, R. C. Hendricks, A study of the effect of multi-g accelleartions on nucleate-boiling ebullition. 1964, National Institute and Space Administration: Lewis Research Center, Ohio.

[16] Y. Y. Hsu, On the size range of active nucleation cavities on a heating surface. Journal of Heat Transfer, 1962. **84**(3).

[17] S. I. Haider, R. L. Webb, A transient micro-convection model of nucleate pool boiling. International Journal of Heat and Mass Transfer, 1997. **40**(15): p. 3675-3688.

[18] T. Yabuki, T. Hamaguchi, O. Nakabeppu, Interferometric measurement of the liquid-phase temperature field around an isolated boiling bubble. Journal of Thermal Science and Technology, 2012. **7**: p. 463-474.

[19] D. Qiu, V. K. Dhir, Experimental study of flow pattern and heat transfer associated with a bubble sliding on downward facing inclined surfaces. Experimental Thermal and Fluid Science, 2002. **26**: p. 605-616.

[20] S. Moghaddam, K. Kiger, Physical mechanisms of heat transfer during single bubble nucleate boiling of FC-72 under saturation conditions-I. Experimental investigation. International Journal of Heat and Mass Transfer, 2009. **52**: p. 1284-1294.

[21] E. J. Owoeye, D. Schubring, CFD Analysis of Bubbble Microlayer and Growth in Subcooled Flow Boiling. Nuclear Engineering Design, 2016. **304**: p. 151-165.

[22] C. Li, N. Koratkar, G. P. Peterson. Bubble Dynamics on Nanostructured Cu Surfaces. in Second International Conference on Integration and Commercialization of Micro and Nanosystems. 2008. Kowloon, Hong Kong.

[23] Y. Nam, J. Wu, G. Warrier, Y.S. Ju Experimental and numerical study of single bubble dynamics on a hydrophobic surface. Journal of Heat Transfer, 2009. **131**(12).

[24] D. Sarker, R. Franz, W. Ding, U. Hampel, Single bubble dynamics during subcooled nucleate boiling on a vertical heater surface: An experimental analysis of the effects of surface characteristics. International Journal of Heat and Mass Transfer, 2017. **109**: p. 907-921.

[25] A. Mukherjee, S.G. Kandlikar, Numerical study of single bubbles with dynamic contact angle during nucleate pool boiling. International Journal of Heat and Mass Transfer, 2007. **50**: p. 127-138.

[26] Y. Yuan, T. R. Lee, Contact Angle and Wetting Properties [Chapter 1]. Surface Science Techniques, 2013.

[27] A. Zou, Fundamentals of microlayer evaporation and its role on boiling heat transfer enhancement, in SURFACE, University Syracuse, Editor. 2015.

[28] H. T. Phan N. Caney, P. Marty, S. Colasson, J. Gavillet, Flow boiling of water in a minichannel: The effects of surface wettability on two-phase pressure drop. Applied Thermal Engineering, 2011. **31**: p. 1894-1905.

[29] Kissa E., Wetting and wicking. Textile Research Journal, 1996. **66**(10): p. 660-668.

[30] H. D. Kim, M. H. Kim, Effect of nanoparticle deposition on capillary wicking that influences the critical heat flux in nanofluids. Applied Physics Letters, 2007. **91**.

[31] J. Kim, S. Jun, R. Laksnarin, S. M. You, Effects of surface roughness on pool boiling heat transfer at a heated surface having moderate wettability. International Journal of Heat and Mass Transfer, 2016. **101**: p. 992-1002.

[32] D. E. Kim, D. I. Yu, S. C. Park, H. J. Kwak, H. S. Ahn, Critical heat flux trigerring mechanism on microstructured surfaces: Coalesced bubble departure frequency and liquid furnishing capability. International Journal of Heat and Mass Transfer, 2015. **91**: p. 1237-1247.

[33] S. H. Kim, H. C. Lee, J. Y. Kang, K. Moriyama, M. H. Kim, H. S. Park, Boiling heat transfer and critical heat flux evaluation of the pool boiling on microstructured surface. International Journal of Heat and Mass Transfer, 2015. **91**: p. 1140-1147.

[34] A. Zou, D. P. Singh, S. C. Maroo, Early evaporation of microlayer for boiling heat transfer enhancement. Langmuir, 2016. **32**: p. 10808-10814.

[35] S. R. Sriraman, Pool Boiing on Nano-Finned Surfaces, University Texas A&M, Editor. 2007.

[36] H. Smrinov, Transport phenomena in capillary-porous structures and heat pipes. 2010: Taylor & Francis Group.

[37] U. Harm, W. Fürbeth, K.-M. Mangold, K. Jüttner, Novel protective coatings for steel based on a combination of self-assembled monolayers and conducting polymers, in Macromolecular Symposia. 2002. p. 65-76.

[38] O. Varlamova, K. Hoefner, M. Ratzke, J. Reif, D. Sarker, Modification of surface properties of solids by femtosecond LIPSS writing: comparative studies on silicon and stainless steel. Applied Physics A, 2017. **123**(725).

[39] P. Goel, A. K. Nayak, P. P. Kulkarni, J. B. Joshi, Experimental study on bubble departure characteristics in subcooled nucleate pool boiling. International Journal of Multiphase Flow, 2017. **89**: p. 163-176.
[40] W. H. McAdams, Heat Transmission. 1942, New York: McGraw-Hill.
[41] Chen J. C., Correlation for boiling heat transfer to saturated fluids in convective flow. Industrial and Engineering Chemistry Process Design and Development, 1966. **5**(3): p. 322-329.
[42] Y. L. Rousselet, Interacting effects of inertia and gravity on bubble dynamics, in Mechanical Engineering. 2014, University of California.
[43] D. Euh, B. Ozar, T. Hibiki, M. Ishii, C.H. Song, Characteristics of Bubble Departure Frequency in a Low-Pressure Subcooled Boiling Flow. Journal of Nuclear Science and Technology, 2010. **47**(7): p. 608-617.
[44] E. W. Washburn, The Dynamics of Capillary Flow. Physical Review, 1921. **17**.
[45] M. S. Plesset, A. Prosperetti, The contribution of latent heat transport in subcooled nucleate boiling. International Journal of Heat and Mass Transfer, 1978. **21**: p. 725-734.

Highlights of the manuscript:

- Surface characteristics effects on bubble waiting periods over vertical heater are studied.
- High resolution imaging techniques captured the life-cycle of a steam bubble.
- Bubble waiting periods are analyzed based on bubble dynamics (bubble sizes, liquid inflow, microlayer evaporation etc.).
- Bubble waiting periods are generally longer over low wetting surfaces.
- For well wetting surfaces, waiting period is shortest for 'optimal roughness height'.